5.5 ENTRAINMENT AND LARGE EDDY STRUCTURE IN CLOUDY BOUNDARY LAYERS

D. C. Lewellen* and W. S. Lewellen
West Virginia University, Morgantown, WV.

1. INTRODUCTION

In previous work (Lewellen and Lewellen, 1998, 2000) we argued that for many quasi-steady buoyantly-driven boundary layers the level of cloud-top entrainment flux realized is equal to the maximum which the large scale eddies can transport across their full depth. In this picture the mean equilibrium entrainment rate is a property of the large-scale circulation, in principle dependent on the large scale circulation structure but independent of the details of the small-scale dynamics within the inversion. This motivated a parameterization for the entrainment rate dependent only on features of the large scale dynamics: a large-eddy entrainment efficiency, closely related to the entrainment parameterization of Stage and Businger (1981).

For some layer dynamics an inverse relation holds as well: the large-scale circulation structure is in part dependent on the magnitude of the entrainment fluxes. For example, Bretherton and Wyant (1997) argued that heating and drying from cloud-top entrainment play a critical role in promoting the "decoupling" transition from a relatively well-mixed stratocumulus layer to a cumulus-coupled layer with more distinct incloud and subcloud circulations, and suggested a diagnostic parameterization for this transition.

In the present work we consider a unified treatment of the feedback between cloud-top entrainment and large-scale circulation structure. Limiting attention to a restricted set of external forcings and a few idealized circulation structures, this allows one to predict, as a function of conveniently chosen input parameters, which circulation structure dominates and what the entrainment fluxes are. These predictions are then tested using an extensive set of large-eddy simulation (LES) results. Derivations, extensions and further discussions may be found in Lewellen and Lewellen (2001).

* Corresponding author address: D. C. Lewellen, MAE Dept. PO Box 6106, WVU, Morgantown, WV, 26506-6106; e-mail: dclewellen@mail.wvu.edu.

2. IDEALIZED TREATMENT

For simplicity we consider boundary layers driven solely by surface heat and moisture fluxes (leaving out any significant radiation, mean wind shear, precipitation, etc.) with the values of those fluxes, the humidity and temperature jumps across the inversion, and the depth of the subcloud layer taken as our basic input parameters. We assume quasi-steady conditions so that the fluxes of conserved quantities are, to a good approximation, linear across the layer.

Starting from three basic eddy scales (full-layer, cloud-layer, subcloud-layer) we define three idealized circulation regimes (I,II,III) depending on which eddy type is hypothesized to limit the entrainment flux transport. In regime I the flux transport is driven by full-layer scale eddies (e.g., as in the dry convective boundary layer). In regimes II and III the entrained flux is transported across the full layer in two steps, first by cloud-scale, then by subcloud-scale eddies. In quasi-steady state the flux transport in the upper and lower circulations equilibrates by weakening the stronger circulation or strengthening the weaker. In II the cloud deck is assumed solid and the entrained flux is the maximum which the upper circulation can support; the subcloud layer is only partially capped with stronger plumes passing through, but with the downward circulation still sufficient to mix the entrained fluxes across that layer. In III (which we associate with a cumulus coupled layer), the subcloud layer transports the maximum entrainment flux it can support (it is effectively capped, behaving as a dry convective layer), while the upper circulation is weakened by a drop in cloud fraction over at least part of the depth of the layer (leading to the appearance of column clouds).

Beginning in regime III and increasing the surface sensible heat flux, for example, augments the lower circulation relative to the upper and a transitional period follows in which the subcloud layer heats and dries faster than the upper layer, reducing the column cloud depth until equilibrium is restored. A big enough change eliminates the column cloud and drives the system into II where the upper circulation has trouble keeping up with the lower; the lower circulation over-

entrains relative to the upper, weakening the capping of the lower layer until equilibrium is restored with the stronger subcloud plumes exiting the layer. With a large enough increase in the surface sensible heat flux the circulation will become organized more into a full-layer circulation and the regime I picture becomes more appropriate.

Denoting the large-eddy entrainment rate limits for the full-layer-scale, cloud-scale, and subcloud-scale eddies as $ENT^{(I)}$, $ENT^{(II)}$, and $ENT^{(III)}$, respectively (where the cloud-scale result is considered for a solid cloud deck), the regimes are determined according to:

$$\begin{aligned} ENT^{(II)} &< ENT^{(I)} &&: \text{regime I} \\ ENT^{(I)} < ENT^{(II)} &< ENT^{(III)} &&: \text{regime II} \\ ENT^{(III)} &< ENT^{(II)} &&: \text{regime III.} \end{aligned} \quad (1)$$

The entrainment in each regime is computed using the large-eddy entrainment efficiency as defined in Lewellen and Lewellen (1998) applied to each idealized circulation. For notational convenience we define "dry" and "wet" contributions to the buoyancy flux, D and W,

$$\overline{w'\theta'_v} \approx \begin{cases} \overline{w'\theta'_l} + L/c_p X_2^d \overline{w'q'_t} & \equiv D \quad \hat{z} < \hat{z}_b \\ X_1^w \overline{w'\theta'_l} + L/c_p X_2^w \overline{w'q'_t} & \equiv W \quad \hat{z}_b < \hat{z} < 1 \end{cases} \quad (2)$$

Here $\hat{z}_b$ is the cloud base height normalized by the inversion height, and we approximate the X's as constants for any given case (typical values X_1^w ≈0.5, X_2^d ≈0.074, and X_2^w ≈0.4) so that D and W are approximately linear.

With this notation the predictions for the "dry" entrainment fluxes, D_i, in each regime are,

$$D_i^{(I)} = -\eta_f D_0 \frac{(1-\hat{z}_b)^2 (W_0/D_0 - 1) + 1}{(1-\hat{z}_b^2)(W_i/D_i) + \hat{z}_b^2} \quad (3)$$

$$D_i^{(II)} = (D_i/W_i) W_0 (\hat{z}_t - 1)/(\hat{z}_t + 1/\tilde{\eta}_c) \quad (4)$$

$$D_i^{(III)} = D_0 [1 - (1+\eta_{sc})/\hat{z}_t] \ , \quad (5)$$

where $\hat{z}_t$ is the subcloud layer depth normalized by the full layer depth. The corresponding "wet" entrainment fluxes are obtained from these by multiplying by the factor (W_i/D_i). The entrainment fluxes W_i and D_i are unknown *a priori*, but their ratio is not: for our idealized conditions this is related to the cloud-top jump ratio, $\zeta \equiv (-L/c_p)\Delta q_t/\Delta\theta_l$, by,

$$W_i/D_i = (X_1^w - X_2^w \zeta)/(1 - X_2^d \zeta) \ . \quad (6)$$

In comparing with LES results below we use values $\eta_f = \eta_{sc} = 0.3$, $\tilde{\eta}_c = 0.5$, for the full-layer-scale, subcloud-scale, and cloud-scale entrainment efficiencies, respectively, based on values found from simulations of dry convective boundary layers with uniform surface heating or spot heating (producing low and high skewness circulations, respectively).

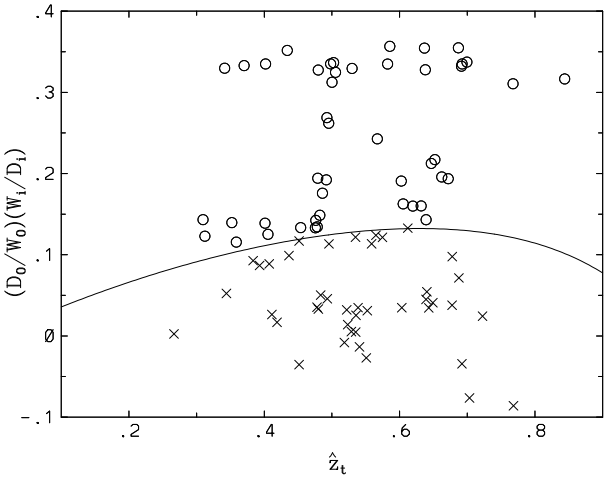

Figure 1: LES results compared with the decoupling boundary prediction of (7) (solid line). Symbols indicate the presence (crosses) or absence (circles) of a column cloud in the simulated cloud fraction profile.

The predicted boundaries between the idealized regime behaviors follow now from (1). Of most interest is the II-III boundary which we associate with the "decoupling" transition leading to a cumulus coupled layer. This we can write in the form,

$$\frac{D_0}{W_0}\frac{W_i}{D_i} \le \frac{\hat{z}_t(1-\hat{z}_t)}{(\hat{z}_t + 1/\tilde{\eta}_c)(1+\eta_{sc}-\hat{z}_t)} \quad \text{for decoupling.} \quad (7)$$

3. COMPARISON WITH LES RESULTS

In fig. 1 we have located LES results (varying surface fluxes, cloud-top humidity and temperature jumps, and cloud depths) on a plot of the left hand side of (7) vs. $\hat{z}_t$, along with the boundary curve defined by (7). Only quasi-steady averages (recognized by approximately linear conserved flux profiles) have been included here. This does not mean that all the cases are steady; some individual simulations with properties such as cloud base height changing in time each contribute several points to fig. 1. The different symbols distinguish between cases found to have column clouds or not, which provides our observational signature for cumulus coupling. The curve defined by (7) does, in fact, do a good job dividing these two populations as predicted. Moreover, the relative depth of the column clouds in regime III was found to grow with increased distance from the boundary with II as expected.

Figure 2 displays the cloud-top entrainment rate

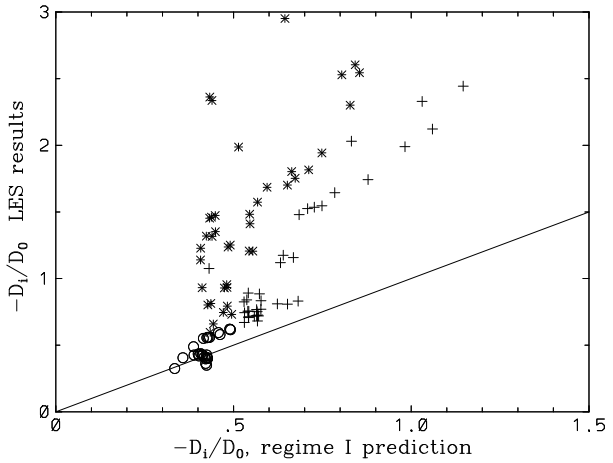

Figure 2: Normalized entrainment flux from LES results vs. regime I prediction from (3). Symbols indicate regimes predicted for the specified boundary layer conditions: I (∘), II (+), and III (*).

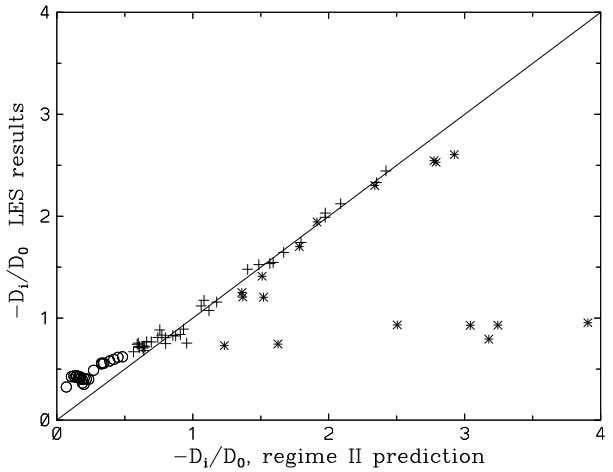

Figure 3: As in fig. 2 but for regime II prediction.

for the LES results vs. the regime I prediction of (3). Figures 3 and 4 show the analogous plots for the regime II and III predictions, (4) and (5), respectively. In each case the measured and predicted values of D_i/D_0 agree well for the subset of the data predicted to be in the corresponding regime, but agree poorly overall with the data sets from the other regimes (some points of which lie off the scale of the given plot). Cases near the predicted II-III or I-II boundaries reasonably satisfy both of the relevant entrainment predictions.

In Lewellen and Lewellen (2001) we did not compute the entrainment efficiency for the upper circulation in regime III, since this requires expressing the buoyancy flux in terms of the conserved fluxes for partly cloudy conditions. Fig. 5 illustrates more recent progress in this direction based on approximating

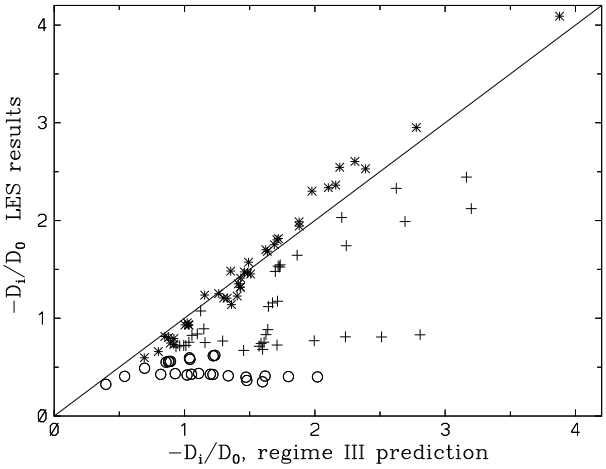

Figure 4: As in fig. 2 but for regime III prediction.

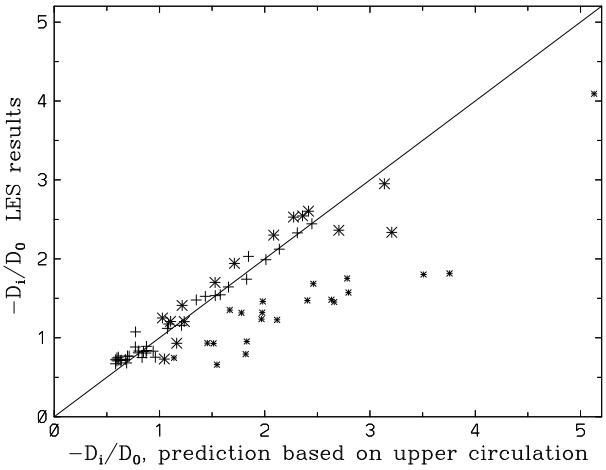

Figure 5: LES entrainment results vs. prediction based on approximate entrainment efficiency computation for cloud-layer circulation. Data from predicted regime II (+) or III (large and small *, the latter where some buoyancy reversal is expected, at least locally, at cloud-top).

$\overline{w'\theta'_v}$ with a linear interpolation between D and W in the column cloud region. Aside from cases with local regions of buoyancy reversal at cloud-top (an effect not incorporated in the entrainment efficiency computation used for the figure) the agreement is quite reasonable. This condition, combined with the prediction in (5), could be used to predict an additional feature such as column cloud height, or used to predict entrainment for transient cases where the upper and lower circulations have not yet equilibrated.

Eq. (7) predicts that the "decoupling" boundary can be traversed via different variations. A cumulus coupled state can be promoted by an increase in surface latent heat flux, decrease in surface sensible heat flux,

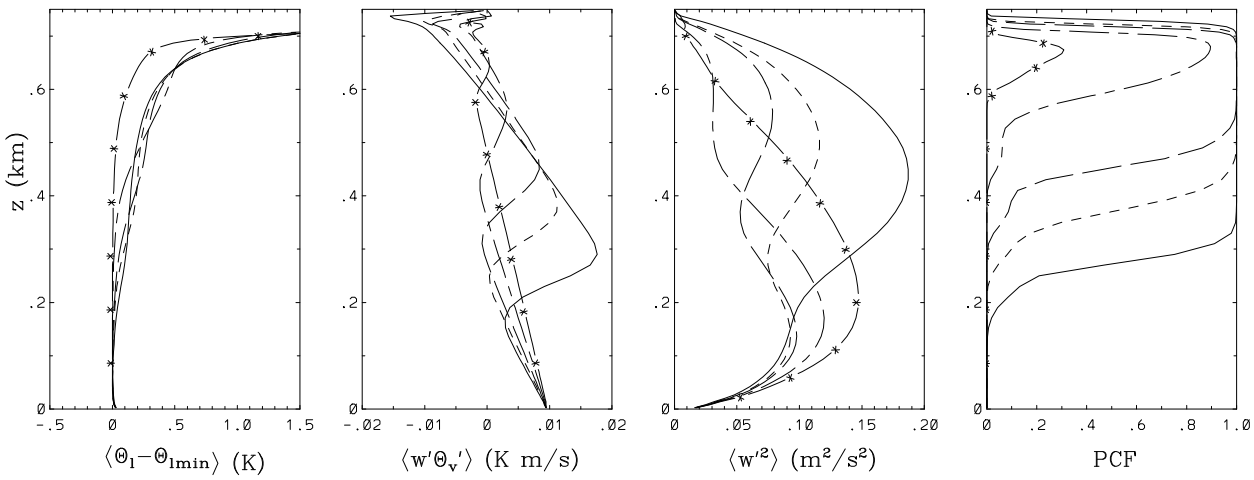

Figure 6: Sample mean vertical profiles for LES case progressing in time from thick cloud to thin. The lines represent two hour averages spaced four hours apart.

or increase in the cloud-top moisture to temperature jump ratio. It may be either promoted or retarded by an increase in the cloud thickness depending on the point in parameter space. We have realized several examples of such transitions via LES, with the location of the crossing of the "decoupling" boundary well predicted by (7).

Fig. 6 shows an example where the layer begins in regime II with a very thick cloud. A uniform drying tendency was added in this case so as to continuously reduce the cloud depth (raising z_t). This drives the system first into regime III but later back into II; the column cloud below the main cloud first grows and then shrinks, accordingly.

4. CONCLUDING REMARKS

The idealized circulations considered obviously represent only very rough caricatures of the fluid dynamics of real boundary layers (or their LES representations). Nonetheless, the resulting model proves relatively successful in predicting transitions between different types of boundary layer dynamics and the resulting changes in entrainment rates this produces. We have considered only a restricted set of boundary layer conditions in this analysis. The inclusion of other effects (some straightforward, others problematic) is discussed in Lewellen and Lewellen (2001) (e.g., the equations are extended to include cloud-top radiative cooling, which can either inhibit or promote decoupling).

5. ACKNOWLEDGEMENTS

This research was supported by a grant from the Office of Naval Research with R. Ferek as technical monitor.

References

Bretherton, C. S., and M. C. Wyant, 1997: Moisture transport, lower-tropospheric stability, and decoupling of cloud-topped boundary layers. *J. Atmos. Sci.*, **54**, 148–167.

Lewellen, D. C., and W. S. Lewellen, 1998: Large-eddy boundary layer entrainment. *J. Atmos. Sci.*, **55**, 2645–2665.

Lewellen, D. C., and W. S. Lewellen, 2000: Boundary layer entrainment for different capping conditions. *Preprints, 14th Symposium on Boundary Layers and Turbulence*, Amer. Meteor. Soc., Aspen, CO, 80-83.

Lewellen, D. C., and W. S. Lewellen, 2001: Entrainment and decoupling relations for cloudy boundary layers. *J. Atmos. Sci.* submitted, available at http://eiger.mae.wvu.edu/cloud.html.

Stage, S., and J. Businger, 1981: A model for entrainment into a cloud-topped marine boundary layer. part I: Model description and application to a cold-air outbreak episode. *J. Atmos. Sci.*, **38**, 2213–2229.